Numerical simulations of three-dimensional transitional compressible flows in turbomachinery cascades

P. De Palma

*Dipartimento di Ingegneria Meccanica e Gestionale (DIMeG),
Centro di Eccellenza in Meccanica Computazionale (CEMeC),
Politecnico di Bari, Bari, Italy*

Abstract

Purpose – This paper aims to provide a validation of a state-of-the-art methodology for computing three-dimensional transitional flows in turbomachinery.

Design/methodology/approach – The Reynolds-averaged Navier-Stokes equations for compressible flows are solved. Turbulence is modeled using an explicit algebraic stress model and $k - \omega$ turbulence closure. A numerical method has been developed, based on a cell-centered finite volume approach with Roe's approximate Riemann solver and formally second-order-accurate MUSCL extrapolation. The method is validated versus two severe test cases, namely, the subsonic flow through a turbine cascade with separated-flow transition; and the transonic flow through a compressor cascade with transitional boundary layers, shock-induced separation and corner stall. For the first test case, the transition model of Mayle for separated flow has been employed, whereas, for the second one, the transition has been modeled employing the Abu-Ghannam and Shaw correlation.

Findings – The comparison of numerical results with the experimental data available in the literature shows that, for such complex flow configurations, an improved numerical solution could be achieved by employing transition models. Unfortunately, the available models are case-dependent, each of them being suitable for specific applications.

Originality/value – A state-of-the-art numerical methodology has been developed and applied to compute very complex flows in turbomachinery. Through an original analysis of the results, the merits and limits of the considered approach have been assessed. The paper points up the fundamental role of transition modeling for turbomachinery flow simulations.

Keywords Finite volume methods, Compressible flow, Turbines, Turbulence, Transition management, Separation

Paper type Research paper

Introduction

Nowadays Computational Fluid Dynamics (CFD) plays a twofold role in the development of modern turbomachinery insofar as it is routinely employed to reduce design time and costs of the components and it is also employed to achieve a deeper understanding of the basic physics of complex flow phenomena which are crucial to design improved engines. Therefore, the validation of the numerical methods and their application to geometries and flow configurations of increasing complexity is of

fundamental interest. The present work provides a validation of a state-of-the-art method for the solution of the Reynolds-Averaged Navier-Stokes (RANS) equation versus two severe three-dimensional test cases involving complex flow phenomena representing a challenge for CFD such as the boundary-layer transition from laminar to turbulent flow and the shock/boundary-layer interaction. The influence of such phenomena on the performance of modern engines is quite relevant: the role of laminar-turbulent transition in gas-turbine engines is nowadays widely recognized (see, e. g. the review of Mayle, 1991), and the shock/boundary-layer interaction problem has been studied for more than 50 years due to its ubiquitous presence in high-speed engine components (Dolling, 2001).

In many turbomachinery flows, although the main stream can be highly turbulent, the boundary layers may be either laminar or turbulent and transition mainly occurs by-passing the "natural" amplification of Tollmien-Schlichting waves due to the typical high level of free-stream turbulence intensity. The performance of turbines (especially low-pressure ones) and compressors can be highly influenced by transition because in many cases such a phenomenon may be crucial for the generation of large separation regions which have a remarkable impact on losses. Therefore, the modeling of transition represents a fundamental issue for the improvement of the performance of modern turbomachinery but it is also a formidable task to achieve because the transition process involves a wide range of scales and it is very sensitive to physical flow features such as pressure gradients (which can be very high in the presence of shocks) and free-stream turbulence, as well as to numerical boundary conditions. The basic mechanism of boundary-layer transition under different flow conditions can be studied using the direct numerical simulation and the large eddy simulation for moderate values of the Reynolds number but, unfortunately, due to their prohibitive computational cost, such techniques are not feasible for the higher Reynolds numbers and complex geometries encountered in most turbomachinery flows. In such cases, a numerical model based on the solution of the RANS equations is needed. Such models are capable of predicting with a good level of accuracy only the mean thermodynamic variables and, in spite of the lack of physical details, they can achieve a good level of reliability for the predictions of specific complex-flow configurations employing turbulence models based on two transport equations. Nevertheless, in spite of the efforts of several researchers aimed at developing low-Reynolds number turbulence models with some built-in transition modeling capability, such models have been proven inadequate for predicting the transition under general flow conditions (Westin and Henkes, 1997; De Palma, 2002). Current research efforts aim at developing transition models based on the concept of intermittency, which represents the fraction of time the flow is turbulent (Mayle, 1991). The most common way to couple the transition model with the turbulence model is to multiply the eddy viscosity coefficient times the intermittency coefficient, even if such a simple approach could produce considerable errors in the calculations of the shear stresses (Mayle, 1991). Moreover, several methods have been proposed to compute the intermittency coefficient, which are based on algebraic correlations (Mayle, 1991; Michelassi *et al.*, 1999) or on the solution of an additional transport equation (Cho and Chung, 1992; Suzen and Huang, 2000; Steelant and Dick, 2001).

During the last years, the author has developed a methodology for the solution of the RANS equations (De Palma *et al.*, 2001), using the low-Reynolds-number $k - \omega$

turbulence model (Wilcox, 1998), which then has been improved (De Palma, 2000) by using the explicit algebraic stress model (EASM) of Gatski and Speziale (1993). The present work describes the extension of the above numerical method to the calculations of separated transitional flows by using the transition criteria proposed by Mayle (1991) and by Abu-Ghannam and Shaw (1980). The three-dimensional compressible flows through a linear turbine cascade and through a linear compressor cascade have been considered. The first test case consists in the subsonic flow through a low-pressure turbine, with separated-flow transition occurring at the rear part of the suction side of the blade. Such a test-case is suitable for validating the separated-flow transition correlation of Mayle (1991). Whereas, the second test case considers the flow through a transonic compressor in which a complex shock/boundary-layer interaction causes the separation of the boundary-layer at the suction side of the blade and a large corner stall. For the simulation of such a flow, the Abu-Ghannam and Shaw (1980) correlation, with Drela's (1995) modification, has been considered to predict the transition onset and the algebraic model proposed in Michelassi *et al.* (1999) has been employed to compute the intermittency coefficient. For both test cases, results obtained employing the EASM, with and without transition model, are compared and validated versus experimental data available in the literature (Hildebrandt and Fottner, 1999; Weber *et al.*, 2001; Kugeler *et al.*, 2001). The reliability of the considered transition models is assessed and the sensitivity of the numerical solution to the transition is investigated.

In the following sections, firstly an overview of the governing equations and of the numerical methodology is given; then a thorough discussion of the flow features is provided together with a critical comparison between numerical and experimental data; finally some concluding remarks are drawn.

Governing equations

The RANS equations, written in terms of Favre mass-averaged variables and using the $k - \omega$ turbulence model (Wilcox, 1998), read:

$$\frac{\partial U}{\partial t} + \frac{\partial \left(F_i^c - F_i^v \right)}{\partial x_i} = S, \tag{1}$$

where U is the vector of the conservative variables:

$$U = \begin{pmatrix} \rho \\ \rho u_i \\ \rho E \\ \rho k \\ \rho \omega \end{pmatrix}, \tag{2}$$

and F_i^c, F_i^v, and S are the components of the convective and viscous fluxes, and the vector of the source terms, respectively:

$$F_i^c = \begin{pmatrix} \rho u_i \\ \rho \delta_{ij} + \rho u_i u_j \\ \rho u_i H \\ \rho u_i k \\ \rho u_i \omega \end{pmatrix}, \tag{3}$$

$$F_i^v = \begin{pmatrix} 0 \\ \hat{\tau}_{ij} \\ b_i \\ (\mu + \sigma^* \mu_t)\frac{\partial k}{\partial x_i} \\ (\mu + \sigma \mu_t)\frac{\partial \omega}{\partial x_i} \end{pmatrix} \tag{4}$$

$$S = \begin{pmatrix} 0 \\ 0 \\ 0 \\ \tau_{ij}\frac{\partial u_i}{\partial x_j} - \beta^* \rho \omega k \\ \frac{\alpha \omega}{k}\tau_{ij}\frac{\partial u_i}{\partial x_j} - \beta \rho \omega^2 \end{pmatrix}. \tag{5}$$

In equations (1-5), u_i are the components of the velocity vector, p and ρ are the pressure and the density, E and H are the specific total internal energy and the specific total enthalpy, respectively, comprehensive of the turbulence kinetic energy, k, and ω is the turbulence specific dissipation rate. Moreover, μ is the dynamic viscosity coefficient, μ_t is the eddy viscosity coefficient, and $\hat{\tau}_{ij}$ is the tensor of the viscous and Reynolds stresses:

$$\hat{\tau}_{ij} = 2\mu\left[\frac{1}{2}\left(\frac{\partial u_i}{\partial x_j} + \frac{\partial u_j}{\partial x_i}\right) - \frac{1}{3}\frac{\partial u_k}{\partial x_k}\delta_{ij}\right] + \tau_{ij}, \tag{6}$$

τ_{ij} being the tensor of the Reynolds stresses, given as:

$$\tau_{ij} = 2\mu_t\left[\frac{1}{2}\left(\frac{\partial u_i}{\partial x_j} + \frac{\partial u_j}{\partial x_i}\right) - \frac{1}{3}\frac{\partial u_k}{\partial x_k}\delta_{ij}\right] - \frac{2}{3}\rho k \delta_{ij}. \tag{7}$$

Finally, the energy fluxes are given as:

$$b_i = u_j\hat{\tau}_{ij} + \left(\frac{\mu}{Pr} + \frac{\mu_t}{Pr_t}\right)\frac{\partial h}{\partial x_i} + (\mu + \sigma^* \mu_t)\frac{\partial k}{\partial x_i}, \tag{8}$$

where Pr and Pr_t are the laminar and turbulent Prandtl numbers, respectively. In the present work, μ is evaluated using Sutherland's law whereas μ_t is computed according

to the low-Reynolds $k - \omega$ turbulence model (Wilcox, 1998), namely, $\mu_t = \alpha^* \rho k/\omega$, the six closure parameters α^* α, β^* β, σ^* and σ being defined as:

$$\alpha^* = \frac{\alpha_0^* + Re_t/R_k}{1 + Re_t/R_k}, \quad \alpha = \frac{5}{9}\frac{\alpha_0 + Re_t/R_\omega}{1 + Re_t/R_\omega}\alpha^{*-1}, \tag{9}$$

$$\beta^* = \frac{9}{100}\frac{5/18 + (Re_t/R_\beta)^4}{1 + (Re_t/R_\beta)^4}, \quad \beta = 3/40, \quad \sigma^* = \sigma = 1/2, \tag{10}$$

$$\alpha_0^* = \beta/3, \quad \alpha_0 = 1/10, \quad R_\beta = 8, \quad R_k = 6, \quad R_\omega = 2.7, \tag{11}$$

where $Re_t = \rho k/\omega\mu$. Finally, the equation of state for perfect gases has been employed to complete the set of the governing equations.

Standard characteristic boundary conditions are imposed at inflow and outflow boundaries, namely: at inlet points, total enthalpy, total pressure, flow angle, turbulence kinetic energy and turbulence specific dissipation rate are imposed whereas the Riemann invariant associated with the outgoing characteristic wave is extrapolated from the computational domain; at outlet points, the pressure is prescribed and the Riemann invariants associated with the outgoing characteristic waves are extrapolated from the computational domain. Furthermore, at solid wall, the no-slip boundary condition is used and the turbulence kinetic energy is set to zero. The pressure and the temperature at the wall are computed by forcing zero normal gradients. Concerning the value of ω at the wall, the following condition has been employed (Menter and Rumsey, 1994): $\omega_w = 60\nu/\beta(\Delta y_w)^2$, where ν is the kinematic viscosity coefficient and Δy_w is the distance between the wall and the first grid point away from the wall. In the present work, non-periodic C-grids are employed, namely the two edges of the branch-cut have a different number of cells. This feature allows to reduce the distortion of the mesh in the blade channel. A conservative treatment of the boundary conditions at the branch-cut is applied by using two rows of phantom cells, overlapping to the grid, in which the dependent variables are evaluated by linear interpolation.

Explicit algebraic turbulence model
The explicit nonlinear constitutive equation, obtained by Gatski and Speziale (1993), has been considered for the Reynolds stress tensor:

$$\tau_{ij} = 2\mu_t\left[S_{ij} - \frac{1}{3}S_{kk}\delta_{ij} + \frac{\alpha_4}{\omega}(S_{ik}W_{kj} + S_{jk}W_{ki}) + \frac{\alpha_5}{\omega}\left(S_{ik}S_{kj} - \frac{1}{3}S_{kl}S_{kl}\right)\right] - \frac{2}{3}\rho k\delta_{ij}, \tag{12}$$

where S_{ij} and W_{ij} are the mean-rate-of-strain tensor and the mean-vorticity tensor, respectively. In equation (12):

$$\mu_t = \rho\alpha^* C_\mu k/\left(C_\mu^0 \omega\right), \tag{13}$$

where:

$$C_\mu = \frac{3(1 + \eta^2)\alpha_1}{3 + \eta^2 + 6\eta^2\xi^2 + 6\xi^2}, \quad C_\mu^0 = 0.09, \quad \eta^2 = \frac{\alpha_2}{\omega^2}(S_{ij}S_{ij}), \quad \xi^2 = \frac{\alpha_3}{\omega^2}(W_{ij}W_{ij}).$$

The closure coefficients α_1-α_5 are evaluated as follows:

$$\alpha_1 = \left(\frac{4}{3} - C_2\right)\frac{g}{2}, \quad \alpha_2 = (2 - C_3)^2\frac{g^2}{4}, \quad \alpha_3 = (2 - C_4)\frac{g^2}{4},$$

$$\alpha_4 = (2 - C_4)^2\frac{g}{2}, \quad \alpha_5 = (2 - C_5)g, \quad g = \frac{1}{0.5C_1 + C_5 - 1},$$

with $C_1 = 3$, $C_2 = 0.8$, $C_3 = 1.75$, $C_4 = 1.31$, $C_5 = 2$. Such values correspond to the pressure-strain correlation model of Launder *et al.* (1975), already employed by Gatski *et al.* (1995) in conjunction with the EASM of Gatski and Speziale (1993).

Transition models

Mayle's model for separated-flow transition

The base mechanism of the separated-flow transition has been described in detail in Mayle (1991). The essential features are shown in Figure 1, which provides a time-averaged representation of the transition region. After flow separation, there is a low-pressure-gradient region (upstream region) followed by a pressure recovery (downstream region). The upstream region is composed by a laminar shear flow, between the abscissae x_s (separation) and x_t (transition onset), and a transition region between the abscissae x_t and x_T (end of transition). At the downstream region, the flow is turbulent and reattaches at x_r. Considering different sets of experimental data, Mayle (1991) proposed the following correlation:

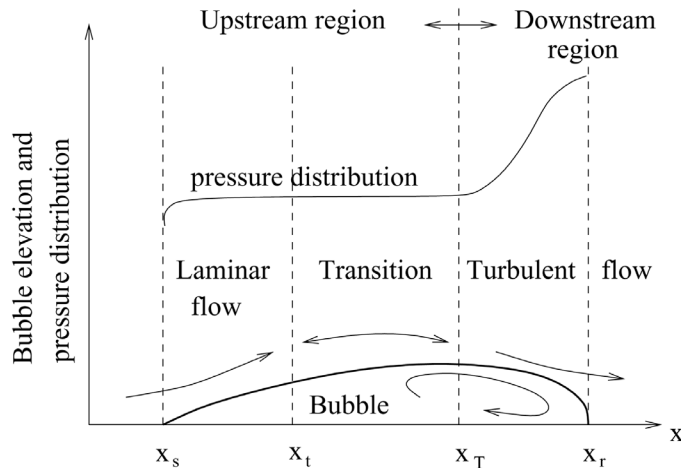$$(Re_x)_{st} = 1,000Re_{\theta s}^{0.7}, \tag{14}$$

Figure 1.
Flow around a separation
bubble from Mayle (1991)

where the Reynolds numbers are defined as:

$$(Re_x)_{st} = \frac{U_s(x_t - x_s)}{\nu_s} \quad \text{and} \quad Re_{\theta s} = \frac{U_s \theta_s}{\nu_s}, \tag{15}$$

U_s, θ_s, and ν_s being the free-stream velocity, the momentum thickness and the kinematic viscosity at the separation point. Using equation (14), it is possible to evaluate the distance between the transition and the separation point, $x_t - x_s$, provided that the conditions at the separation point are known. Furthermore, Mayle provides a second experimental correlation:

$$(Re_x)_{LT} = \frac{U_s(x_T - x_t)}{\nu_s} = 400 Re_{\theta s}^{0.7}, \tag{16}$$

which enables to estimate the length of the transition region, $x_T - x_t$. In such a region the intermittency factor, I, is evaluated as:

$$I = 1 - \exp\left[-0.412 \frac{(x - x_t)^2}{(x_{75} - x_{25})^2}\right], \tag{17}$$

where x_{25} and x_{75} correspond to the locations where I is equal to 0.25 and 0.75, respectively, and $I = 0.99$ corresponds to the abscissa x_T (Mayle, 1991). Inserting such a value in equation (17), and knowing $(x_T - x_t)$ from equation (14), the difference $(x_{75} - x_{25})$ is evaluated. Therefore, for transitional-flow computations, the eddy viscosity is defined as $\mu_{\text{tran}} = \mu_t$. Equation (17) is an experimental correlation due to Dhawhan and Narasimha (1958) which describes the growth of turbulence near walls. In the present work no attempt has been made to improve the model recalibrating the above correlation for each turbulence model employed. Finally, concerning the iteration procedure employed in the present work, the computations start with the intermittency factor equal to zero everywhere. At the beginning, the flow separates from the blade surface near the trailing edge. Knowing the flow characteristics at the separation point, i.e. U_s, θ_s and ν_s, it is possible to compute x_t, using the correlation equation (14), and the length of transition, $x_T - x_t$, from the correlation equation (16). Iterating, the separation point shifts upstream along the suction side until it reaches a stable location; hence, the separation bubble, transition point, and transition length become stable.

Model based on the correlation of Abu-Ghannam and Shaw
The correlation of Abu-Ghannam and Shaw (1980) is based on the evaluation of the Reynolds number:

$$Re_\theta = \frac{\theta u_\infty}{\nu}, \tag{18}$$

where θ is momentum thickness of the boundary layer, ν is the kinematic viscosity and u_∞ is the local velocity magnitude at the edge of the boundary layer. It is noteworthy that, in this calculations, the edge of the boundary layer is defined as the first point from the wall at which the magnitude of the velocity varies less then 1 percent. According to the correlation proposed by Abu-Ghannam and Shaw (1980), modified in Drela (1995), the transition model evaluates a critical value, $Re_{\theta,t}$, which indicates the location of the transition onset, as:

$$Re_{\theta,t} = 163 + 74.3\left[0.55\tanh\left(\frac{10}{H} - 5.5\right)\right](0.94n_{\text{crit}} + 1), \tag{19}$$

where H is the shape factor of the boundary layer and:

$$n_{\text{crit}} = -8.43 - 2.4\ln\left(\frac{Tu}{100}\right), \tag{20}$$

accounts for the influence of the free-stream turbulence intensity, $Tu = 100\sqrt{2k/3u_\infty^2}$. Finally, the intermittency function, I, which is employed to compute the eddy viscosity coefficient, $\tilde{\mu}_t$, in transitional flow calculations, namely:

$$\tilde{\mu}_t = I\mu_t, \tag{21}$$

is evaluated using the expression proposed in Michelassi *et al.* (1999) as:

$$I = \left(\frac{25}{25 + 275\left(1 - \sin\frac{\pi}{2}\left(\frac{Re_\theta - Re_{\theta,t}}{Re_{\theta,t}}\right)\right)}\right)^\alpha, \tag{22}$$

where $\alpha = 3$ for the present computations.

It is noteworthy that, for the three-dimensional-flow configurations considered in this work, the above transition models have been employed at each spanwise location considering the flow as two-dimensional.

Numerical method
The Navier-Stokes equations are discretized by a cell-centred finite-volume method employing structured grids. The numerical convective fluxes at each cell interface are evaluated using a flux difference splitting approach based on Roe's approximate Riemann solver. The left and right states of the Riemann problems are reconstructed using a formally second-order-accurate fully upwind MUSCL extrapolation. The min-mod limiter function is employed in order to damp spurious oscillations. The diffusive terms are evaluated by second-order-accurate central differencing. Time discretization is based on an explicit (four stage) Runge-Kutta scheme with coefficients: $\alpha_1 = 1/4$, $\alpha_2 = 1/3$, $\alpha_3 = 1/2$. Moreover, in order to accelerate the convergence towards the steady-state solution, three well known methods are used, namely: local time stepping, implicit residual smoothing and multigrid strategy. Such a procedure allows the use of $CFL = 3$ for the present test cases. In particular, a standard FAS multigrid strategy (Brandt, 1982) is employed to drive the residual of the governing equations towards machine zero. A V-cycle has been used, with three grid levels. Linear interpolations are employed to transfer the corrections from each coarse grid to the finer one.

Turbine cascade
The three-dimensional flow through the linear turbine cascade T106, has been considered, the blade having a typical midspan profile of a low-pressure turbine rotor (see Hildebrandt and Fottner (1999) for geometrical details). The flow is subsonic with isentropic exit Mach number equal to 0.59 and Reynolds number, based on the chord

length, c, and on exit conditions, equal to 5×10^5; the inlet flow angle with respect to the axial (ax) direction is equal to 37.7°. Steady-flow computations have been performed with inlet turbulence intensity equal to 5.8 percent and inlet turbulence length scale is equal to $0.02c$ in order to compare the results with the experimental data reported in Hildebrandt and Fottner (1999). Moreover, the measured (Hildebrandt and Fottner, 1999) total-pressure spanwise profile has been prescribed at inlet points. The computational domain (half span) has been discretized using a C-grid with $384 \times 40 \times 48$ cells, which has been selected with a grid-refinement analysis and provides grid-converged results. The average non-dimensional distance of the first cell center from the blade surface is about $y^+ = 1$, whereas at the sidewall $y^+ = 2$. Two set of results are provided, obtained without and with the transition model of Mayle (1991). Figures 2 and 3 show the contours of the loss coefficient defined as $\zeta = (p_{t1} - p_t)/(p_{t1} - p_2)$, where p_t is the total pressure and the subscripts 1 and 2 indicate inlet and outlet conditions, respectively. These figures refer to a plane located at $x/c_{ax} = 1.5$, the value of ζ corresponding to each contour level being shown in Figure 3. Figure 2 provides the experimental data (Hildebrandt and Fottner, 1999); the distribution of the loss coefficient clearly shows a large two-dimensional flow-region at midspan and is characterized by three loss cores. The principal one (LC1) originates between the suction side branch of the horseshoe vortex and the passage vortex; the loss core LC2 is directly related to the passage vortex, whereas the third loss core, LC3, is due to the counter-rotating corner-vortex induced by the passage vortex in the corner between the sidewall and the suction side (Hildebrandt and Fottner, 1999). All these features are well captured by both numerical solutions shown in Figure 3. It noteworthy that both computations overestimate the losses, nevertheless, employing the transition model, the local peak value of the loss coefficient in the wake ($\zeta = 0.12$) is closer to the experimental data ($\zeta = 0.09$). For the same plane located at $x/c_{ax} = 1.5$, Figure 4 shows the spanwise distributions of the pitchwise-averaged exit flow angle,
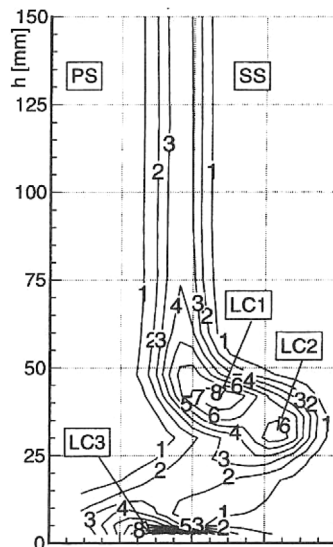

Figure 2. Loss-coefficient contours ($\Delta\zeta = 0.03$) : experimental data (Hildebrandt and Fottner, 1999)
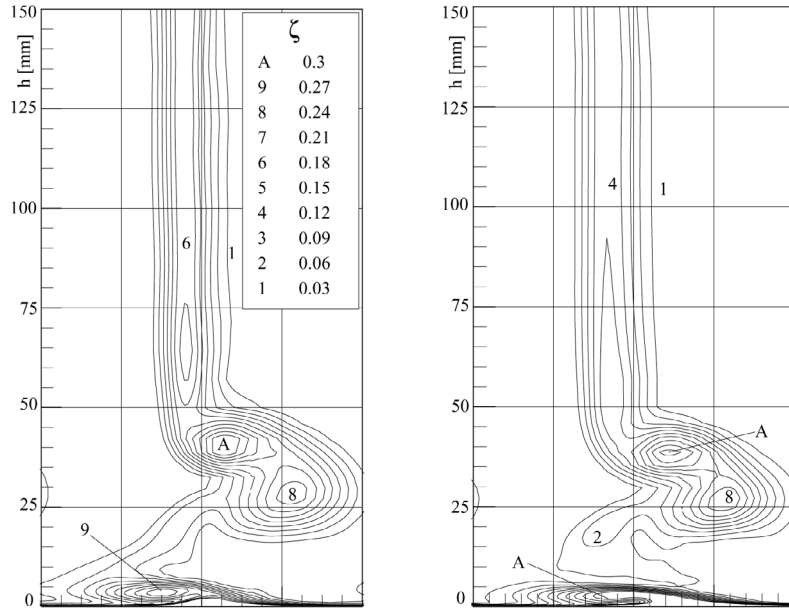
Figure 3.
Loss-coefficient contours
($\Delta\zeta = 0.03$) : fully
turbulent flow
computations (left) and
transitional flow
computations (right)

$\beta_2 = \arctan(u/v)$ (u and v being the axial and pitchwise velocity components, respectively), versus the non-dimensional spanwise coordinate, z/s, s being the blade span (300 mm). Both numerical results agree quite well with the experimental data of Hildebrandt and Fottner (1999).

Finally, Figure 5 shows two three-dimensional views of the stream traces close to the suction-side surface of the blade, computed employing the EASM without and with transition, respectively. The main difference between the two solutions is the separation bubble is clearly detected when employing the transition model. Both solutions show the evolution of the passage vortex and of the suction-side branch of the horseshoe vortex along the suction surface. Furthermore, the transitional-flow
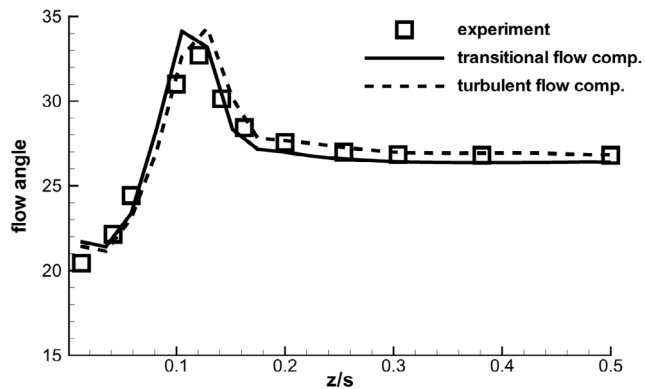
Figure 4.
Spanwise distributions of
the averaged flow
angle, β°_2
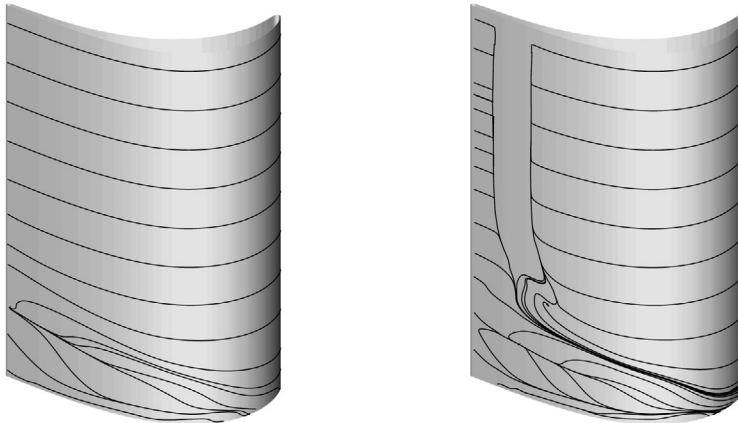
computation also shows that the suction side leg of the horseshoe vortex interacts with the separation bubble. This is a typical flow configuration for low-pressure turbine cascades in which high-loss fluid is fed into the separation bubble whereas the rest is convected downstream with the vortex.

Compressor cascade

The transonic flow through a linear compressor cascade has been considered, with low flow-turning and a strong shock wave at the blade passage inlet. The geometry of the cascade and the test conditions have been provided by DLR together with the experimental data obtained using the transonic wind tunnel at DLR-Cologne (Weber *et al.*, 2001; Kugeler *et al.*, 2001). The test condition considered in the present work corresponds to inlet Mach number equal to 1.09 at midspan, inlet flow angle equal to 147.1° and Reynolds number, based on the chord length and inlet flow conditions, equal to 1.9×10^6. The inlet endwall boundary-layer profile, measured at $x/c = 0.85$ ahead of the leading edge, has been also provided by DLR. For the numerical simulation, the total pressure, the total temperature and the flow angle are prescribed at inlet points, whereas the value of the static pressure is assigned at outlet points in order to match the inlet Mach number. Furthermore, at inlet points, turbulence intensity equal to 1 percent and mixing length equal to 1 percent of the chord are imposed. The computational domain (half span) has been discretized using a structured C-grid with $320 \times 48 \times 48$ cells. Such a grid has been selected with a grid-refinement analysis and provides grid-converged results.

The average non-dimensional distance of the first cell center from the blade surface, y^+, is about equal to one, whereas at the endwall $y^+ \simeq 3$.

Three computations have been performed:

(1) a fully-turbulent-flow (FTF) computation;

(2) a first transitional-flow (TF1) computation, employing the Abu-Ghannam and Show transition model;

(3) a second transitional-flow (TF2) computation, forcing an abrupt transition just behind the shock.

Experimental evidence that there is a laminar shock-induced separation motivates the latter TF2 computation. It is noteworthy that, the transition criterion of Mayle (1991), which was designed for flows without shocks, cannot be employed for this test case because it leads to a large separation at the suction side. Furthermore, also due to the presence of the bow shock ahead of the blade which contributes to amplify the turbulence level, the free-stream turbulence intensity inside the blade channel is always greater than 0.6 percent, therefore, it appears reasonable to employ the by-pass transition model of Abu-Ghannam and Show. Table I shows the pitchwise-averaged values at midspan of the static pressure ratio, p_2/p_1 of the exit Mach number, M_2, and of the exit flow angle, β_2, defined as $\beta = \arctan(v/u) + 90°$, u and v being the axial and pitchwise velocity components, respectively. Section 1 is located at $x/c_{ax} = -0.25$, ahead of the cascade, whereas section 2 is at $x/c_{ax} = 1.43$, downstream of the cascade. Table I provides a comparison between experimental and computed results which demonstrates the good level of accuracy achieved for such averaged predicted values. Figure 6 shows the Mach number contours at midspan, computed employing the Abu-Ghannam and Shaw transition model. Such a figure shows that, due to the supersonic inflow velocity, a shock wave is generated at the inlet of the cascade which impinges on the suction side of the blade, interacting with both the blade and the endwall boundary layers. Figures 7-9 show the three-dimensional views of the

Table I.
Average exit angle, exit
Mach number and static
pressure ratio, at
midspan

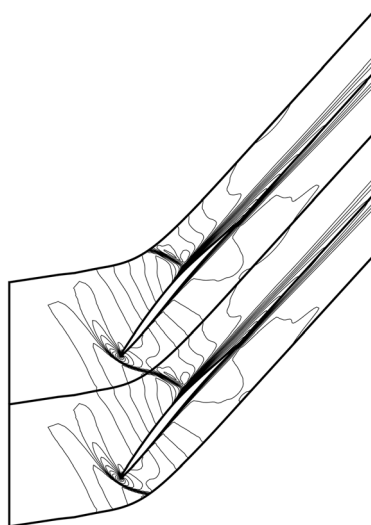|	exp.	FTF	TF1	TF2
p_2/p_1	1.45	1.414	1.438	1.438
M_2	0.7014	0.7039	0.715	0.716
β_2	136.5°	137.6°	137.1°	136.8°

Figure 6.
Transitional flow (TF1):
Mach number contours at
$z/h = 0.5$ ($\Delta M = 0.05$)

isentropic Mach number contours at the wall. In all computations, the shock is sharper at midspan and moves upstream from midspan towards the endwall, in agreement with the experimental data (Weber *et al.*, 2001).

Nevertheless, the computed curvature of the shock is slightly overestimated in all calculations. In fact, Figure 10, which shows the numerical and measured isentropic Mach number distributions along the blade at the spanwise section corresponding to $z/h = 0.071$, shows that, for transitional flow computations, the position of the shock is slightly shifted towards the leading edge; whereas, Figure 11, which refers to midspan ($z/h = 0.5$), shows a good agreement with the experimental data for all computations. However, TF2 provides a better agreement with respect to the experiments in the region of higher Mach number. Experimental data clearly show a flattening of the isentropic Mach number distribution around the peak value which is due to the laminar shock-induced separation. Concerning the computations, on one
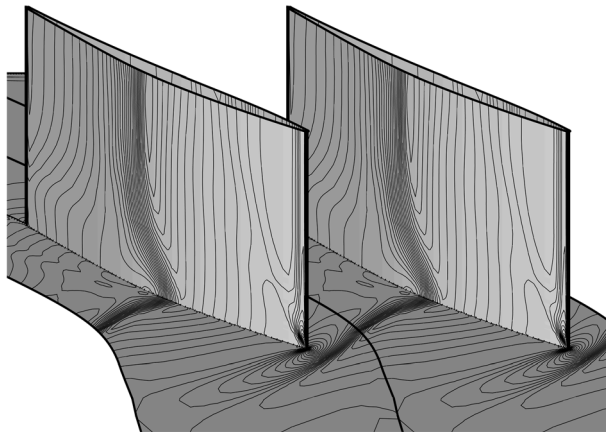
Figure 7.
Turbulent flow: isentropic Mach number contours at wall ($\Delta M_{is} = 0.02$)
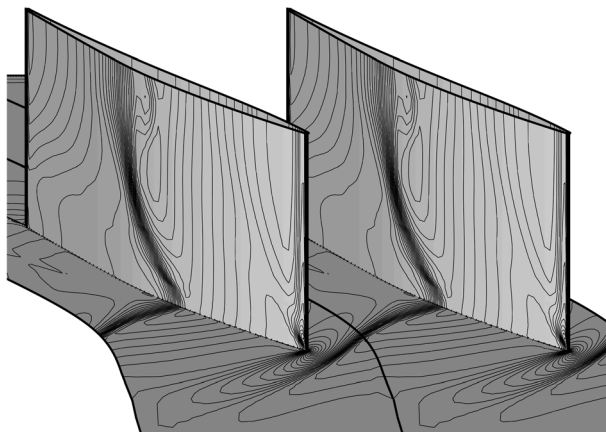
Figure 8.
Transitional flow (TF1): isentropic Mach number contours at wall ($\Delta M_{is} = 0.02$)
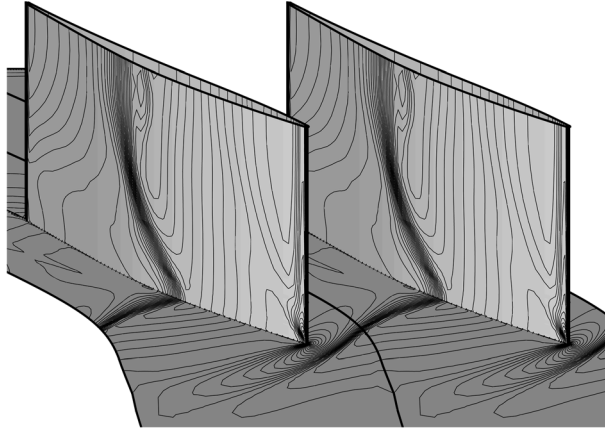
Figure 9.
Transitional flow (TF2):
isentropic Mach number
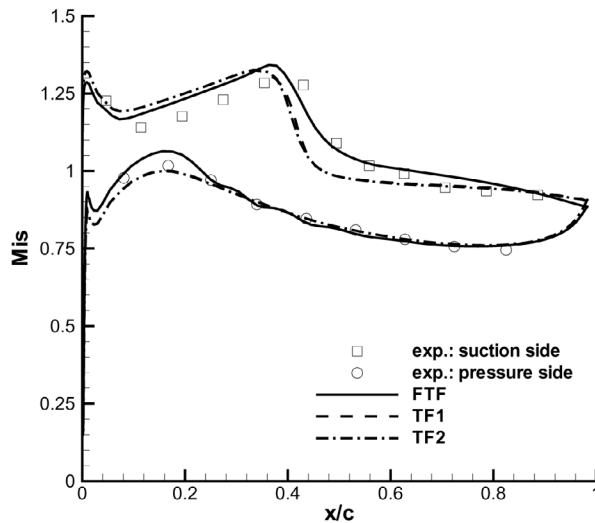contours at wall ($\Delta M_{is} = 0.02$)

Figure 10.
Isentropic Mach number
distribution along the
blade $z/h = 0.071$

hand, for the FTF computation the suction-side boundary-layer is completely turbulent; on the other hand, for the TF1 computation the transition is predicted ahead of the shock, so that in both cases a shock/turbulent-boundary-layer interaction is computed. This explains the discrepancy between experimental and numerical data in the region where the shock impinges on the suction side. Such a behavior is confirmed by the TF2 computation: forcing the transition just behind the shock wave improves the corresponding numerical solution – see the dashed-dot line in Figure 11 – in the region of the shock/boundary-layer interaction, providing a reduced Mach number peak which is very close to the experimental data.

The numerical results indicate the presence of a separation bubble induced by the shock, as shown by the stream traces at the suction side of the blade shown in
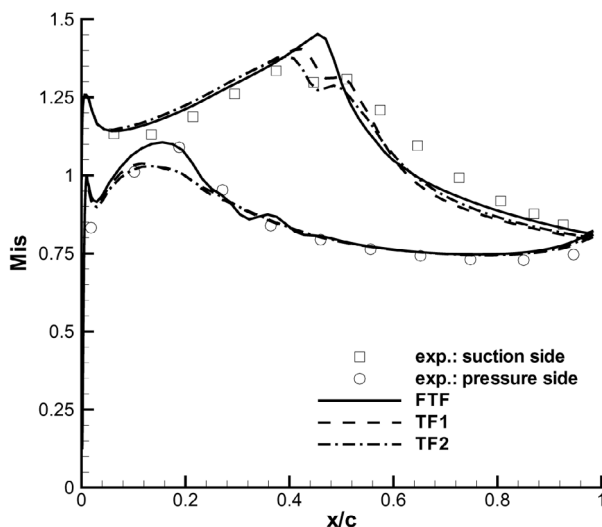
Figure 11.
Isentropic Mach number
distribution along the
blade at $z/h = 0.5$

Figures 12-14. The extension of the bubble is in good agreement with the experimental data shown in Figure 15, which show separation from 49 to 69 percent of the chord. All numerical results show a shorter bubble: from 55 to 72 percent, from 52 to 68 percent and from 50 to 68 percent of the chord, for the FTF, TF1 and TF2 computations, respectively. Figures 12-14 also show the structure of the shock-induced corner stall which reasonably agrees with the oil streak lines shown in Figure 15.

The computed total pressure (p_t) contours at the axial plane located at $x/c_{ax} = 0.86$ (inside the blade passage) are shown in Figures 16 and 17. They can be compared with the experimental distribution of the total pressure at the same location (Weber *et al.*, 2001), shown in Figure 18. From such figures it is possible to notice the extension of the low-total-pressure region and of the wake which are in good agreement with the experimental data. It is noteworthy that the transitional-flow computations can predict the reduction of the boundary-layer thickness in the spanwise direction
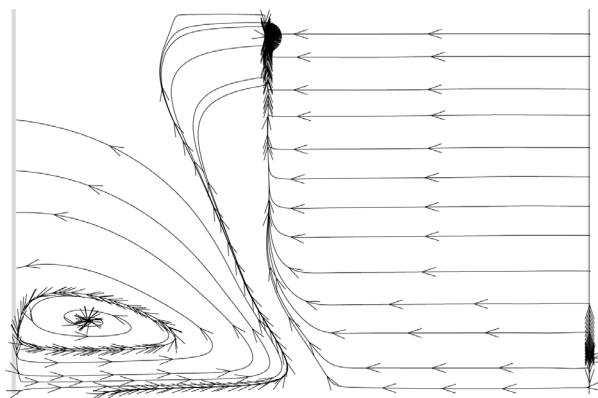

Figure 12.
Turbulent flow: stream
traces close to the wall

Figure 13.
Transitional flow (TF1):
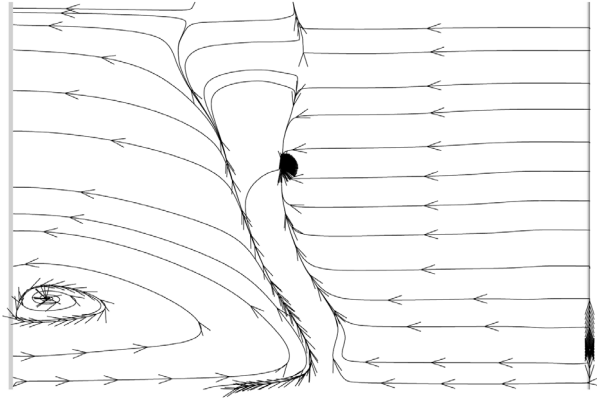stream traces close to the
wall

Figure 14.
Transitional flow (TF2):
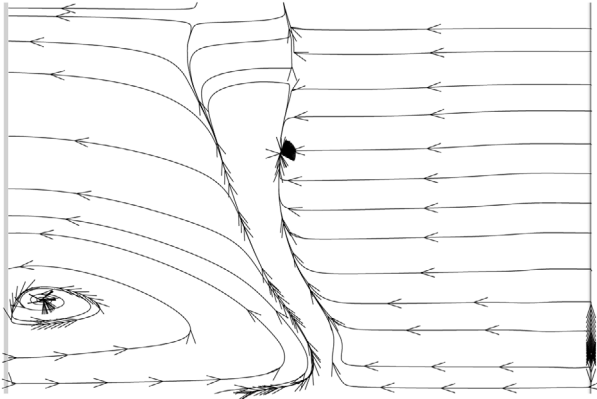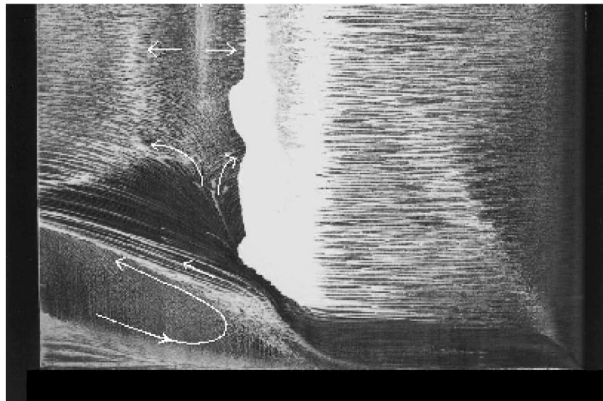stream traces close to the
wall

Figure 15.
Oil streak lines at the
suction side (Weber *et al.*,
2001)

close to the corner stall. The result obtained forcing the transition (TF2) is not shown
because it is very close to Figure 17.

Figures 19 and 20 show the spanwise distributions of the average
total-pressure-loss coefficient, $\omega = (p_{t1} - p_t)/(p_{t1} - p_1)$, and the average flow angle,
β_2, at a plane located at $x/c_{ax} = 1.43$, downstream of the cascade. For both
experimental (Weber et al., 2001) and numerical results, mass, momentum and energy
are averaged in the pitchwise direction at each spanwise location. The loss coefficient
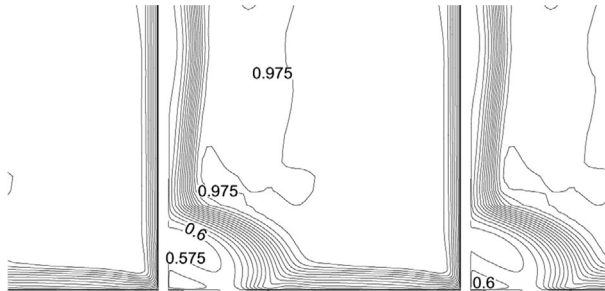
Figure 16.
Turbulent flow: total
pressure contours at
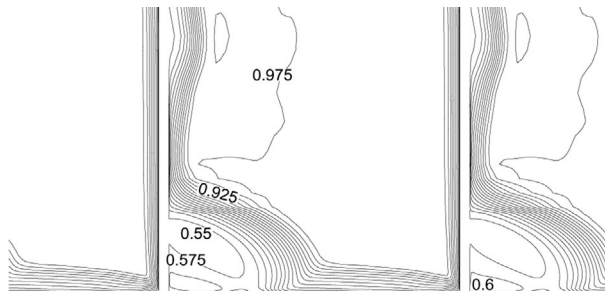$x/c_{ax} = 0.86 \ \Delta(p_t/p_{t1} =$
$0.025)$

Figure 17.
Transitional flow (TF1):
total pressure contours at
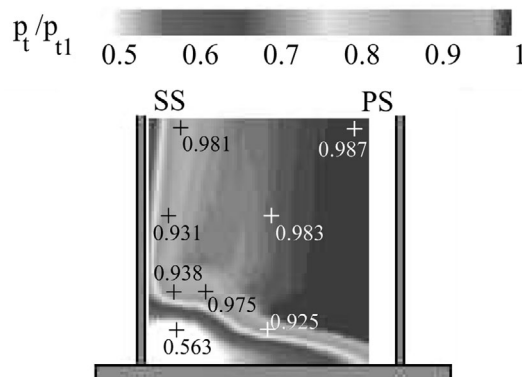$x/c_{ax} = 0.86, \ \Delta(p_t/p_{t1} =$
$0.025)$

Figure 18.
Total pressure
distribution at $x/c_{ax} =$
0.86 : experimental data
(Weber et al., 2001)
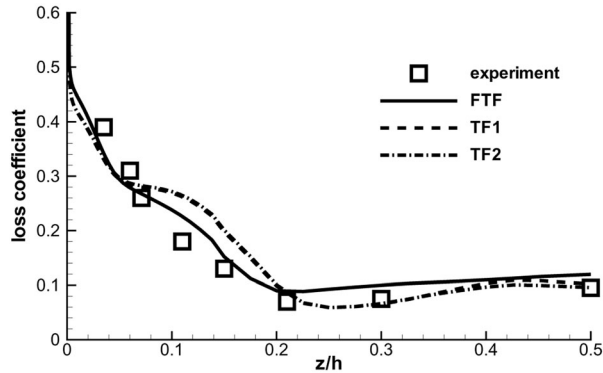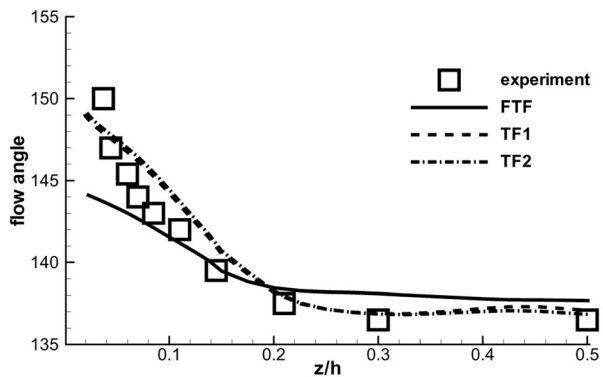
slightly decreases from midspan ($z/h = 0.5$) to $z/h = 0.2$ and than it increases approaching the endwall. Numerical results predict quite well such a behavior and are in a good quantitative agreement with the experimental data, as also shown in Table II which provides the values of ω at four spanwise locations, for completeness. The flow angle, β_2, shows a continuous increase towards the endwall. This is the typical behavior of highly staggered cascade in which the separation of the boundary layer at the endwall suppresses the classical overturning due to the crossflow from pressure side to suction side. The oil-flow picture at the endwall, provided in Weber *et al.* (2001) and shown in Figure 21, clearly demonstrates the high deviation of the flow around the trailing edge with the formation of a separation line and a focus close to the rear part of

	exp.	FTF	TF1	TF2
$z/h = 0.071$	0.26	0.265	0.28	0.28
$z/h = 0.15$	0.13	0.15	0.197	0.2
$z/h = 0.3$	0.075	0.1	0.066	0.066
$z/h = 0.5$	0.095	0.12	0.1	0.095
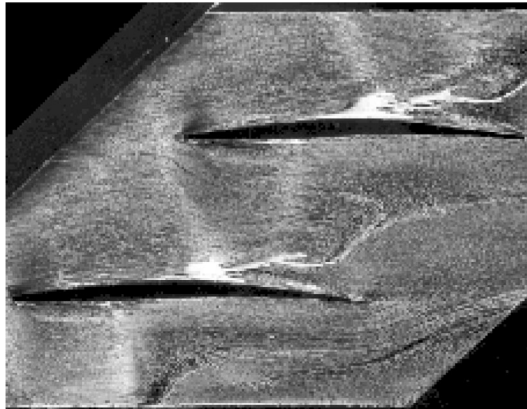
the suction side. The stream traces obtained with the TF1 computation, shown in
Figure 22, show a very similar behavior, the location of the focus being predicted quite
accurately.

Concluding remarks

A state-of-the-art methodology for computing three-dimensional compressible viscous
flows has been validated versus two severe test cases. Computations are based on the
solution of the RANS equations with $k - \omega$ turbulence closure and an explicit algebraic
stress model. Furthermore, two models for laminar-turbulent boundary-layer
transition have been considered, namely, the one for separated-flow transition due to
Mayle and the Abu-Ghannam and Shaw model. The governing equations have been
discretized in space by a cell-centred finite-volume method based on Roe's flux
difference splitting, with second-order-accurate upwind space discretization. Explicit
Runge-Kutta time integration has been employed together with residual smoothing
and a multigrid strategy to accelerate convergence towards steady-state.

The first test case consists in the subsonic flow through a low-pressure turbine, with
separated-flow transition occurring at the rear part of the suction side of the blade.
Computations demonstrate that only using a sufficiently accurate transition model it is
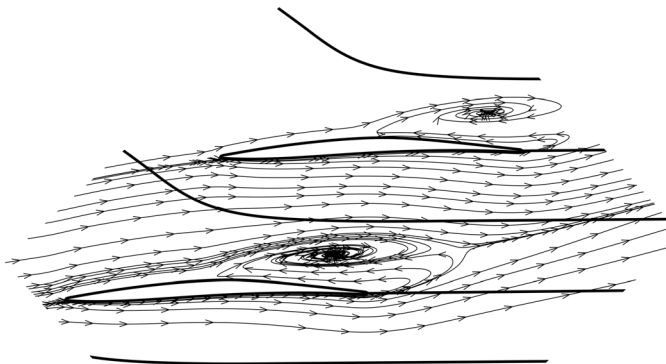
possible to capture the suction-separation bubble. Furthermore, transitional-flow calculations provide an improved prediction of the loss-coefficient distribution downstream of the cascade with respect to fully turbulent calculations.

The second test case considers the flow through a transonic compressor cascade in which a complex shock/boundary-layer interaction causes the separation of the boundary-layer at the suction side of the blade and a large corner stall. Three calculations have been performed:

(1) without transition model (fully-turbulent-flow calculation);

(2) with transition model; and

(3) forcing *ad hoc* the transition.

The results have been compared with the experimental data available in the literature, a good prediction of the general properties of the flow being achieved. Nevertheless, some discrepancies with respect to the experimental data have been highlighted concerning the local behavior of the flow close to the separation bubble at the suction side of the blade. Such a separation is induced by the shock impinging on the suction side. The calculations show that the fully-turbulent-flow computation does not predict correctly the shock/laminar-boundary-layer interaction so that the peak value of the isentropic Mach number and the length of the separation bubble differ from the experimental data. The use of the Abu-Ghannam and Shaw transition model only slightly improves the solution, because transition is predicted too early, before the shock. Finally, computations performed forcing *ad hoc* the transition demonstrate that the present numerical method can provide a solution closer to the experimental data in the shock/boundary-layer interaction region. This confirms that the discrepancies between numerical and experimental data are essentially due to the inadequacy of the transition model.

The results provided in the present paper indicate that, for such complex flow configurations, an improved numerical solution could be achieved by employing transition models. Unfortunately, the available models are still too much case-dependent, and each of them is suitable for specific applications. The development of improved transition models, suitable for a wide range of flow configurations, remains a formidable task to be pursued in the future. At this purpose, more detailed and accurate experimental data, together with LES and DNS results, will be crucial to gain further knowledge of the basic mechanism of transition.

References

Abu-Ghannam, B.J. and Shaw, R. (1980), "Natural transition of boundary layers – the effect of turbulence, pressure gradient and flow history", *Journal of Mechanical Engineering Science*, Vol. 22 No. 5, pp. 213-28.

Brandt, A. (1982), "Guide to multigrid development", *Lecture Notes in Mathematics*, Vol. 960, Springer Verlag, Berlin, pp. 220-312.

Cho, R. and Chung, M.K. (1992), "A k-ε-γ equation turbulence model", *J. Fluid Mech.*, Vol. 237, pp. 301-22.

De Palma, P. (2000), "Numerical simulation of transitional turbomachinery flows", in Satofuka, N. (Ed.), *Computational Fluid Dynamics 2000*, Springer, New York, NY, pp. 449-54.

De Palma, P. (2002), "Accurate numerical simulation of compressible turbulent flows in turbomachinery", *AIAA Journal*, Vol. 40 No. 4, pp. 702-8.

De Palma, P., Pascazio, G. and Napolitano, M. (2001), "Accurate and efficient solutions of unsteady viscous flows", *Int. J. Num. Meth. Heat and Fluid Flow*, Vol. 11 No. 4, pp. 286-307.

Dhawhan, S. and Narasimha, R. (1958), "Some properties of boundary layer flow during transition from laminar to turbulent motion", *J. Fluid Mech.*, Vol. 3, pp. 418-36.

Dolling, D.S. (2001), "Fifty years of shock-wave/boundary-layer interaction research: what next?", *AIAA Journal*, Vol. 39 No. 8, pp. 1517-31.

Drela, M. (1995), "MISES implementation of modified Abu-Ghannam/Shaw transition criterion", *MIT Aero-Astro*, February.

Gatski, T.B. and Speziale, C.G. (1993), "On explicit algebraic stress models for complex turbulent flows", *J. Fluid Mech.*, Vol. 254, pp. 59-78.

Gatski, T., Abid, R. and Rumsey, C. (1995), "Prediction of nonequilibrium turbulent flows with explicit algebraic stress models", *AIAA Journal*, Vol. 33 No. 11, pp. 2026-31.

Hildebrandt, T. and Fottner, L. (1999), "A numerical study of the influence of grid refinement and turbulence modeling on the flow field inside a highly loaded turbine cascade", *ASME Journal of Turbomachinery*, Vol. 121, pp. 709-16.

Kugeler, E., Weber, A. and Lisiewicz, S. (2001), "Combination of a transition model with a two-equation turbulence model and comparison with experimental results", *Proceedings of the 4th European Conference on Turbomachinery, Fluid Dynamics and Thermodynamics*, Firenze, pp. 877-87.

Launder, B.E., Reece, G.J. and Rodi, W. (1975), "Progress in the development of a Reynolds stress turbulence closure", *J. Fluid Mech.*, Vol. 68, pp. 537-66.

Mayle, R.E. (1991), "The role of laminar-turbulent transition in gas turbine engines", *ASME Journal of Turbomachinery*, Vol. 113, pp. 509-37.

Menter, F.R. and Rumsey, C.L. (1994), "Assessment of two-equation turbulence models for transonic flows", AIAA Paper, 94-2343.

Michelassi, V., Martelli, F., Dénos, R., Arts, T. and Sieverding, C.H. (1999), "Unsteady heat transfer in stator-rotor interaction by two-equation turbulence model", *ASME Journal of Turbomachinery*, Vol. 121, pp. 436-47.

Steelant, J. and Dick, E. (2001), "Modeling of laminar-turbulent transition for high freestream turbulence", *Journal of Fluids Engineering*, Vol. 123, pp. 22-30.

Suzen, Y.B. and Huang, P.G. (2000), "Modeling of flow transition using an intermittency transport equation", *ASME Journal of Fluids Engineering*, Vol. 122, pp. 273-84.

Weber, A., Schreiber, H-A., Fuchs, R. and Steinert, W. (2001), "3D transonic flow in a compressor cascade with shock induced corner stall", ASME paper 2001-GT-345, New Orleans.

Westin, K.J.A. and Henkes, R.A.W.M. (1997), "Application of turbulence models to bypass transition", *ASME Journal of Fluids Engineering*, Vol. 119, pp. 859-66.

Wilcox, D.C. (1998), *Turbulence Models for CFD*, 2nd ed., DCW Industries, Inc., La Canada, CA.

Corresponding author
P. De Palma can be contacted at: depalma@poliba.it